



## **My Adventures at DESY Hamburg**

Arne Zantop, Georg-August Universität Göttingen, Germany

20th September 2016



We study the local translational order and the bond orientational order of a system of charge stabilized colloidal suspensions via Monte Carlo simulations. Specifically, we use a potential model that simulates hard-core non-overlapping colloids with a screened Coulomb repulsion. We show that structure factors obtained from simulations are in very good accordance with the experimentally measured structure factors of charge stabilized suspensions of poly-acrylate spheres, and also match the analytically derived structure factors from the Derjaguin-Landau-Verwey-Overbeek (DLVO) theory. Charge stabilized suspensions exhibit clustering - amorphous and short-range crystallinity - behaviour at higher concentrations. In this study, our goal is to investigate how the typical real-space structural order parameters behave for different concentrations of the colloids and salt concentrations. Finally, we present corresponding radial distribution functions, bond orientational order maps and structure factors of different systems that would be useful in X-ray scattering measurements for these charge stabilized suspensions.

# Contents

<b>1</b>	<b>Introduction</b>	<b>1</b>
1.1	Interaction between colloids . . . . .	1
1.2	DLVO Theory and interaction potential . . . . .	2
<b>2</b>	<b>Methods</b>	<b>3</b>
2.1	Statistical physics and it's simulation . . . . .	3
2.2	Structural properties . . . . .	6
2.2.1	Radial Distribution Function and Structure Factor . . . . .	6
2.2.2	Bond orientational order parameters . . . . .	8
<b>3</b>	<b>Results</b>	<b>11</b>
3.1	Comparing to experimental data . . . . .	11
3.2	Further investigation of local correlation . . . . .	12
3.2.1	Radial distribution function . . . . .	12
3.2.2	Bond orientational order . . . . .	14
3.3	Structure factor . . . . .	17
<b>4</b>	<b>Conclusion and outlook</b>	<b>19</b>
	<b>References</b>	<b>20</b>

# 1 Introduction

Mesoscopic colloids of different types, suspended in a solvent, are ubiquitous in our everyday life. Examples range from large molecules or proteins in our bodies to micelles in soaps, paints and other industrial products. Hence, research is of interest for both fundamental sciences and applied science. Using X-rays one can directly measure the local distance correlations (on an average) between any two colloid particles in a system. The relationship between the measured intensity data in reciprocal space and real-space structural metrics is well understood. However, the exact effect of local orientational order or symmetry on the structure factor is not clear. In this work we shall shed some light on these effects.

## 1.1 Interaction between colloids

The solvent molecules are typically much smaller than the colloids, so that colloids exhibit brownian motion. As they have been described so far, colloids would only interact via Van der Waals attractive forces arising from fluctuating dipole moments. Since the thermal energy  $k_B T$  is typically smaller than this interaction energy, one has to employ some stabilisation strategy to prevent irreversible aggregation of the solvate. There are generally two types stabilisation strategies of colloids, both of which introduce repulsions between any two colloids, namely those being charge stabilised and those stabilised by steric effects. In the case of charge stabilisation, the surface of colloids is covered by ionisable chemical groups which ionise when dissolved in a polar liquid.

The colloids then possess a net surface charge of several hundred, up to  $10^5$ , unit charges. A schematic drawing of such a colloid is presented in figure 1. This net surface leads to a coulomb repulsion of colloids. Even without the counterions the polarisable liquid will screen the potential due to polarisation.

In the solvent around a colloid an atmosphere of counterions forms, which also screens the potential. This so called double layer, drawn in red and green in fig. 1, has a thickness of the Debye screening length  $\lambda_D$ . The interpenetration of those layers leads to a repulsion between colloids which has a Coulomb part multiplied with exponential decay.

Following the other strategy, the colloids surfaces are covered by a layer of polymer chains. When these overlap when particles are close, the polymer's entropy gets reduced, which also results in a repulsive force that stabilises the system.

Both these interactions can be tuned by adding salt ions in the first case or polymers or smaller colloids in the other case. This renders the interaction more short ranged, which is also called a screening. In the case of charge

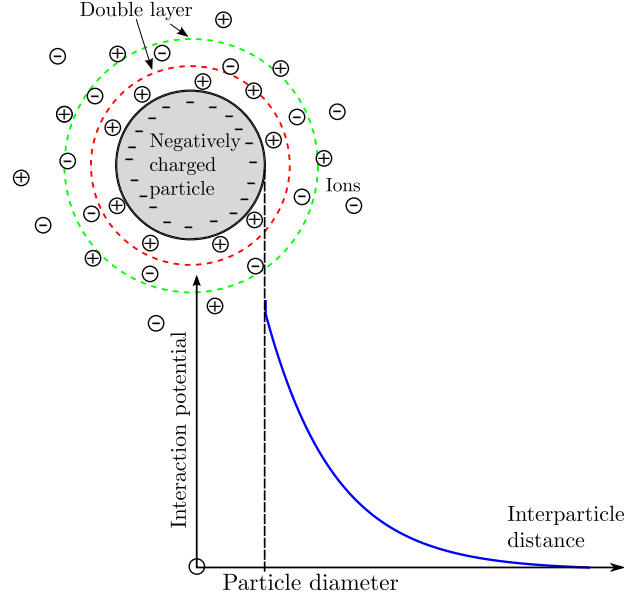


**Figure 1:** Schematic of a charged colloid in a polar solvent with ions.

stabilisations the ions shield the colloid's charge and the interaction decays faster.

## 1.2 DLVO Theory and interaction potential

The DLVO theory yields a pair potential for the interaction of colloidal suspensions of charge stabilised particles having a double layer of counterions, using a mean-field approximation in the limit of low surface potentials. The result is a hard-core Yukawa, i.e. screened coulomb, potential;

$$u(\mathbf{r}_{ij}) = \begin{cases} \infty, & |\mathbf{r}_{ij}| < 1 \\ \frac{u_0}{\beta} \frac{e^{-\kappa|\mathbf{r}_{ij}|}}{|\mathbf{r}_{ij}|}, & \text{else,} \end{cases} \quad (1)$$

where the surface potential or coupling strength

$$u_0 = \frac{\lambda_B}{\sigma} \left( \frac{e^{\kappa/2}}{1 + \kappa/2} \right)^2 Z^2$$

and the screening parameter

$$\kappa^2 = \frac{\lambda_B/\sigma}{1 - \phi} (24\phi|Z| + 8\pi n_s \sigma^3),$$

with the Bjerrum length  $\lambda_B = \beta e^2/(\epsilon\epsilon_0)$ , the solvent's relative dielectricity  $\epsilon$ , unit charge  $e$ , number of charges  $Z$  and the reciprocal temperature

$\beta = (k_B T)^{-1}$  [1]. The volume fraction is given by  $\phi = \pi/6 n \sigma^3$  with the number density  $n$ . As we can see, the volume fraction  $\phi$  also influences the screening. This is simply due to the fact that the more space the colloids take, the less space is left for the ions. This can be thought of as leading to a higher effective salt concentration.

Due to the nature of the interaction, involving an atmosphere of counterions, we have to consider contributions of many body interactions to the pair potential. A way to account for the shielding is the use of a small cutoff radius of ca. the gap after the first liquid's neighbour shell, after which the interaction is not considered any more. To make the resulting potential continuous, a shift subtracting the potential's value at cutoff can be done. Though, in the case of a colloidal particle lying between two others, between which the potential is considered, this might not be physical. The investigation of whether this is the case or not is also part of this work.

For the simulations we will show later we used the parametrisation as in table 1.

Quantity	Value
particles $N$	3375
temperature	293 °K
configurations	1000
size $\sigma$	223.4 nm
cutoff	2.5 $\sigma$
charge $Z$	400
$\epsilon$	80

**Table 1:** Simulations' parameters

We simulated various volume fractions between  $\phi_{\min} = 0.16$  and  $\phi_{\max} = 0.5011$  at two salt concentrations  $n_s = 0.1$  mM and  $n_s = 0.01$  mM.

## 2 Methods

### 2.1 Statistical physics and its simulation

As we will see, the DLVO theory provides a very good analytical prediction of shape of the structure factor. It doesn't provide the structural information in which we are interested, though, with an analytical approach. We can overcome this limitation with numerical simulations using the Monte-Carlo technique. With Monte-Carlo integration of the phase space distribution function, we don't have to consider velocities of particles, but this

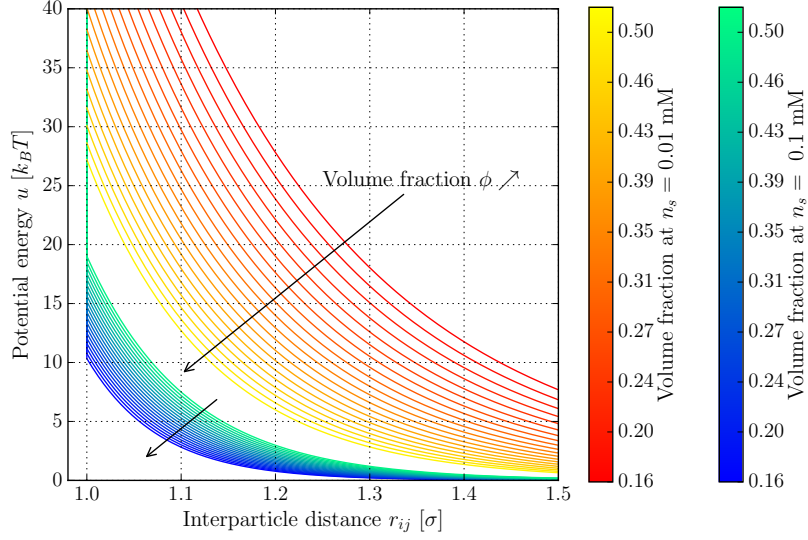


**Figure 2:** Plot of the interaction potentials used in this work. The red/yellow curves are for the lower salt concentration  $n_s = 0.01$ . The blue/green curves are for the higher salt concentration  $n_s = 0.1$ , the two colour codes give the volume fraction at each salt concentration. We see the lower screening as the red/yellow decay more slowly than the blue/green ones.

also means that there is no possibility to calculate any dynamical properties with the sampled configurations.

Physical systems consist of huge numbers, typically several  $6 \times 10^{23}$  (Mols), of particles. To simulate such large numbers of particles is even with todays computers not feasible. In order to obtain reliable results for the materials properties in bulk anyway, it is common practice to circumvented this complication with the use of periodic boundary conditions. The interaction between each pair of colloids is calculated according to the nearest periodic image convention.

As mentioned before, our goal is now to obtain the ensemble average value of an observable. Using the familiar calculus of statistical mechanics this means calculating the mean value of that observable  $\langle O(\mathbf{\Gamma}) \rangle$  under the phase space distribution function  $\rho(\mathbf{\Gamma})$  of interest for all possible configurations  $\mathbf{\Gamma}$ . This means evaluating the integral

$$\langle O \rangle = \int \rho(\mathbf{\Gamma}) O(\mathbf{\Gamma}) d\mathbf{\Gamma}. \quad (2)$$

The number possible states is infinite, so that one needs an efficient way to sample in order to make the integral converge with a finite number of sample configurations  $\mathbf{\Gamma}_i$ . This is done via the Metropolis scheme. One generates a Markov chain of particle configurations  $\mathbf{\Gamma}_i$  following the transition



probability for a configuration  $\mathbf{\Gamma}_i$  to a configuration with a small random modification  $\mathbf{\Gamma}_{i+1}$ , given by the distribution function. This has the great advantage, that the partition sum doesn't have to be calculated. The solvent can be considered to be a incompressible, so having a constant volume fraction of the solute, we have an isothermal isochoric ensemble and the transition probability is given by Boltzmann factor

$$p_{\text{transition}}(\mathbf{\Gamma}_i, \mathbf{\Gamma}_{i+1}) = \frac{\rho(\mathbf{\Gamma}_{i+1})}{\rho(\mathbf{\Gamma}_i)} = e^{-\beta\Delta E},$$

The first configuration in this Markov chain is either generated randomly or as a crystal lattice. This method needs to equilibrate, so in order to get a good estimate of the Integral 2, a sufficiently large number of the first generated configurations are not considered.

Another possibility to evaluate the phase space distribution function might generally be the direct simulation of molecular dynamics in the classical approximation, in the present case of mixed hard and soft body interactions this is difficult though. The treatment of hard bodies' collisions requires the exact collision time to compute the momentum transfer. An improved estimate, compared to collision tracing in during velocity integration, can be obtained with a variable step width integration. Further, also multi body collisions have to be considered. With regards to this huge necessary efforts, following a Monte-Carlo scheme is much more convenient [2].

## 2.2 Structural properties

For the investigation of the liquid structure, we numerically calculate the radial distribution function (RDF), the static structure factor, and a set of bond orientational order parameters (BOOs). In the following, we give a brief introduction of those measures for the properties of liquids.

### 2.2.1 Radial Distribution Function and Structure Factor

Fluids, in contrast to ideal gases, possess short range spatial correlations. Those can be expressed with the two particle density, additional to the one particle density function. This density function describes the probability of finding a particle at  $\mathbf{r}'$  if there is a particle at  $\mathbf{r}$ ;

$$\rho_N^{(2)}(\mathbf{r}, \mathbf{r}') = \left\langle \sum_{i \neq j} \delta(\mathbf{r} - \mathbf{r}_i) \delta(\mathbf{r}' - \mathbf{r}_j) \right\rangle, \quad (3)$$

where the sum goes over all pairs of particles. In other words, it gives the average density distribution a particle of the system would see around itself [3].

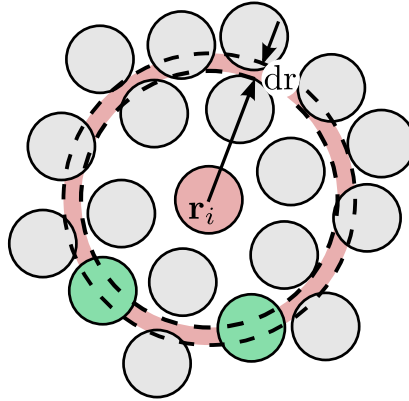


**Figure 3:** The radial distribution function (eq. 4) gives the probability of finding another particle (green) in the volume element  $4\pi r^2 dr$  at distance  $r$  (red circle) from a particle  $i$  (red), in the case of an homogeneous and isotropic liquid. We can see that inside the red region, there is naturally a distance of increased probability for other particles. This results in a peak in  $\rho_N^{(2)}(r)$ , called the first neighbour shell, a typical feature of liquids.

If the system is both homogeneous and isotropic, this function only depends on the scalar distance between particles

$$\rho_N^{(2)}(r) = \left\langle \sum_{i \neq j} \delta(r - |\mathbf{r}_i - \mathbf{r}_j|) \right\rangle = g_N^{(2)}(r) \rho, \quad (4)$$

with the density  $\rho$  and the pair distribution function  $g_N^{(2)}(r)$ , which is, in the present case of homogeneity and isotropy of the liquid, called radial distribution function.

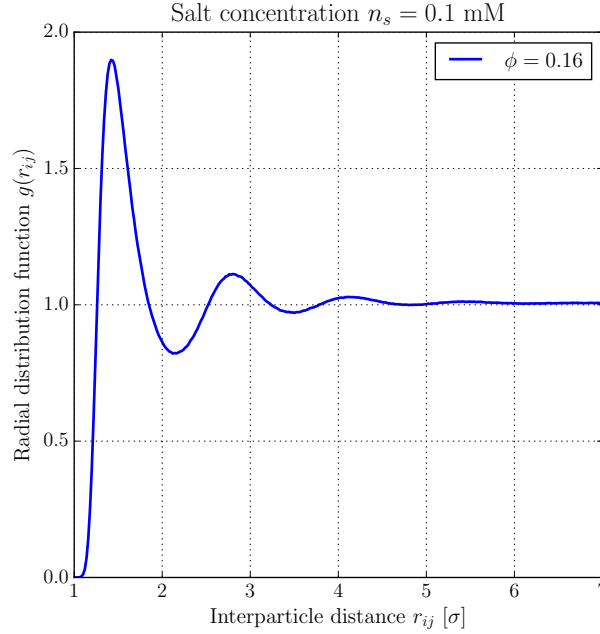


**Figure 4:** The radial distribution function for the hard-core Yukawa model given by eq. 1 parametrized as in table 1. Between 1 and 2, we see the increase caused by the first neighbour shell. As we go to larger separation, we also see the typical decay to unity, which means the density the particle  $i$  sees is just the average density for large distances.

Like for crystals, this correlations can be observe via diffraction patterns with the difference that, since there is no regular lattice in fluids, the diffraction patterns do not exhibit sharp peaks. X-ray and neutron diffraction experiments therefore can be performed in order to yield equilibrium static structure properties. The way incident light is spatially scattered into a pattern by a material is mathematically described by the static structure factor, which can be defined as the Fourier density correlation

$$S(\mathbf{k}) = \frac{1}{N} \left\langle \sum_{i=1}^N e^{i\mathbf{k}\mathbf{r}_i} \sum_{j=1}^N e^{i\mathbf{k}\mathbf{r}_j} \right\rangle = 1 + \frac{1}{N} \left\langle \sum_{i \neq j}^N e^{i\mathbf{k}(\mathbf{r}_i - \mathbf{r}_j)} \right\rangle,$$

with the number of particles  $N$  and the momentum transfer  $\mathbf{k}$ . Conveniently expressed for the computation from simulation's structural

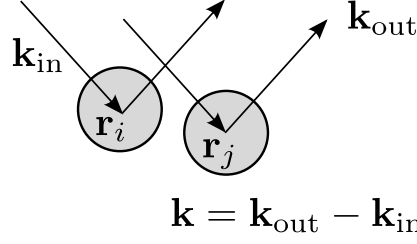


**Figure 5:** The structure factor describes the scattering of a wave due to the inter particles' distance correlations, which results in a path difference.

data[4] is the form

$$S(\mathbf{k}) = \frac{1}{N} \left\langle \left| \sum_{i=1}^N \cos(\mathbf{k} \cdot \mathbf{r}_i) \right|^2 + \left| \sum_{i=1}^N \sin(\mathbf{k} \cdot \mathbf{r}_i) \right|^2 \right\rangle. \quad (5)$$

The wave vector  $\mathbf{k}$ 's components need to be multiples of  $2\pi/L_i$ , where  $L_i$  is the respective box side length of the finite simulation box. The structure factor as in eq. 5 can be visualised radially averaged as  $S(|\mathbf{k}|)$ .

Another way to compute the structure factor is to directly calculate it from the radial distribution function as

$$S(k) = 1 + 4\pi\rho \int_0^\infty \frac{\sin(kr)}{kr} (g(r) - 1) r^2 dr, \quad (k \neq 0).$$

where  $g(\mathbf{r})$  is the RDF. While the density describes the probability of finding a particle in a region of space, the radial distribution function describes the probability of finding a second particle at the separation  $\mathbf{r}$  of a reference particle.

Compared to the structure factor, the radial distribution has the advantage of its clear physical meaning and simplicity of visualising it.

### 2.2.2 Bond orientational order parameters

So far we have dealt with distance correlation between pairs of particles. The advantage here is that one can arrive at these results from both experiments and simulations of particles with pairwise interaction, which provides a method to model the actual interaction of particles. From configurations produced with simulations, we can though calculate some more quantities. We are interested in the local symmetry in the first neighbour shell of particles, which can easily be understood in a 2D plane like in figure 7. If a

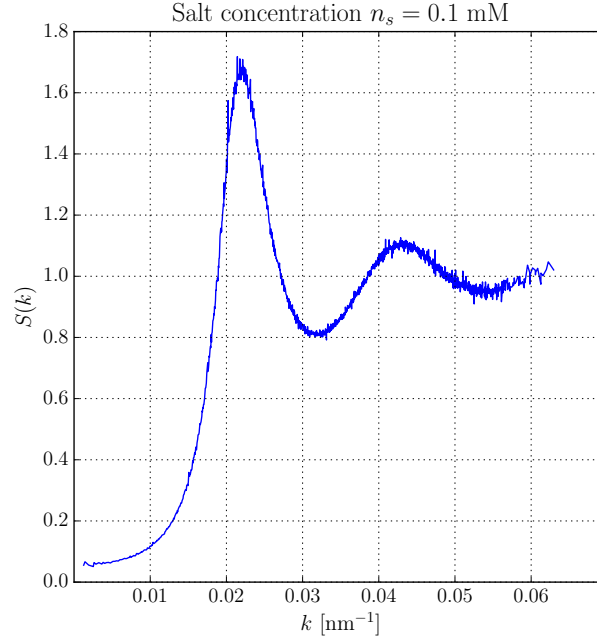


**Figure 6:** Structure factor for the same state  $\phi = 0.16$  as in fig. 4, calculated according to eq. 5, thus a typical liquid's structure factor. The peak slightly above  $0.02 \text{ nm}^{-1}$  is produced by the high distance correlation of the first neighbour shell.

particle has six neighbours (green colour) and between the connecting lines to the centre particle (red colour) the angle  $\theta$  is  $60^\circ$  each, one observes a perfect 6-fold symmetry. In 3 dimensions, the  $l$ -fold order of particle  $i$  with nearest neighbours  $j \in \text{NN}(i)$ , is defined with  $l$ -order spherical harmonics  $Y_{lm}(\theta_{ij}, \varphi_{ij})$  so that [5]

$$q_l(i) = \left[ \frac{4\pi}{2l+1} \sum_{m=-l}^l \left| \underbrace{\frac{1}{|\text{NN}(i)|} \sum_{j \in \text{NN}(i)} Y_{lm}(\theta_{ij}, \varphi_{ij})}_{q_{lm}(i)} \right|^2 \right]^{1/2}.$$

These parameters vary between zero and unity for none and perfect symmetry, respectively. What should be emphasised at this point is, that these order parameters contain no information of how far particles are from each other. Since the volume fraction changes, the code that calculates this quantities always calculates the minimum after the first peak in the RDF and considers all particles within this distance of a particle as its next neighbours. In a liquid, these symmetries can be present, even if the system is not a crystal. To see crystal structures and local crystal-like arrangements,

one can compare particles'  $q_l(i)$  to the values of a perfect crystal. To have a measure of how much crystalline a sample is, we can calculate the correlation between the the  $l$ -fold bond order of different particles  $i$  and  $j$  via

$$c_l(ij) = \frac{\sum_{m=-l}^l q_{lm}(i) \overline{q_{lm}(j)}}{\left[ \sum_{m=-l}^l |q_{lm}(i)|^2 \right]^{1/2} \left[ \sum_{m=-l}^l |q_{lm}(j)|^2 \right]^{1/2}}.$$

This quantity varies between -1 for perfect anticorrelation and 1 meaning perfect correlation [5].

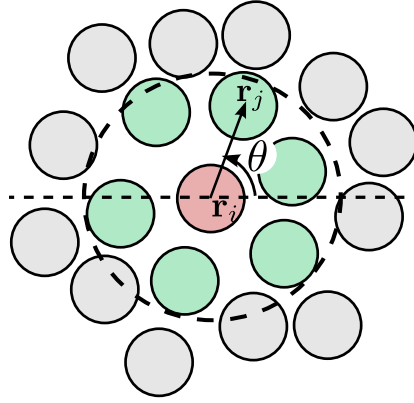


**Figure 7:** Schema of how the bond order parameters work in 2 dimensions. Here we don't have a perfect 6-fold symmetry in the first neighbour shell (green particles), but an increased one.

From the experimental side, related information can be acquired with X-ray cross correlation analysis (XCCA). For the scattering Intensity  $I(q, \varphi)$  this is

$$c(q, \Delta) = \frac{\langle I(q, \varphi) I(q, \varphi + \Delta) \rangle_{\varphi} - \langle I(q, \varphi) \rangle_{\varphi}^2}{\langle I(q, \varphi) \rangle_{\varphi}^2}.$$

The exact connection between the bond orientational order parameters and XCCA is though not known, but is of interest because of the bond orientational order parameter's clear meaning.

### 3 Results

#### 3.1 Comparing to experimental data

We can compare our simulations' results with experimental scattering data[6], that was kindly provided by F. Westermeier. For this comparison we used the fitting parameters of the analytical treatment provided by Westermeier and his coauthors in [6]. The plots for different salt concentrations at the two volume fractions  $\phi = 0.16$  and  $\phi = 0.32$  are shown in fig. 8 and fig. 9, respectively.

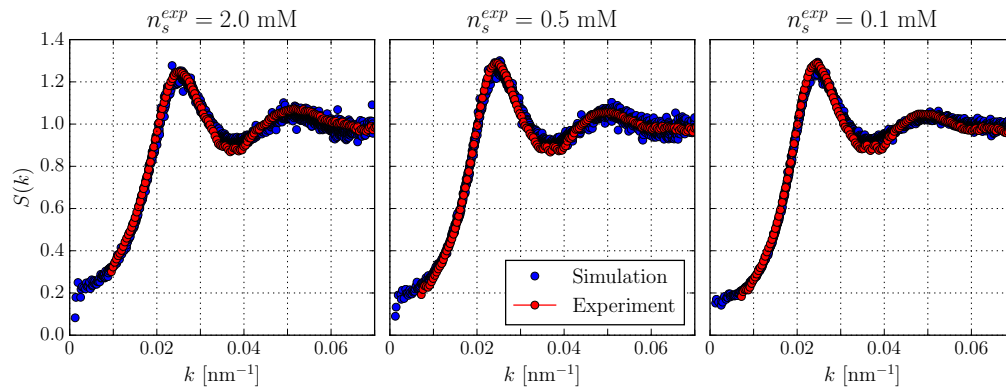


**Figure 8:** Structure factors at volume fraction  $\phi^{\text{nom}} = 0.16$ .

We can see that the two differently obtained curves are overlapping well. For this lower volume fraction we get a maximum root mean square deviation of 3%.

Salt concentration $n_s$	RMS
0.1	0.027
0.5	0.024
2.0	0.023

**Table 2:** RMS at volume fraction  $\phi^{\text{nom}} = 0.16$ .

For the higher volume fraction in fig. 9 we see a good overlap, although the maximum root mean square deviation is now around 5% here. In the results for this volume fraction, we can see the effect of increased screening as salt concentration increases. The leftmost panel in fig. 9 shows the least salt concentration. As we look at the other two panels, from left to right, we see the local correlation between particles increase, since the first peak - produced by the first neighbour shells - increases. We can also see that

### 3.2 Further investigation of local correlation

the correlations, and with it the interaction, become more long ranged. This feature is also demonstrated by the structure factors, where greater oscillations are also present at high values of the momentum transfer ( $q$ ).

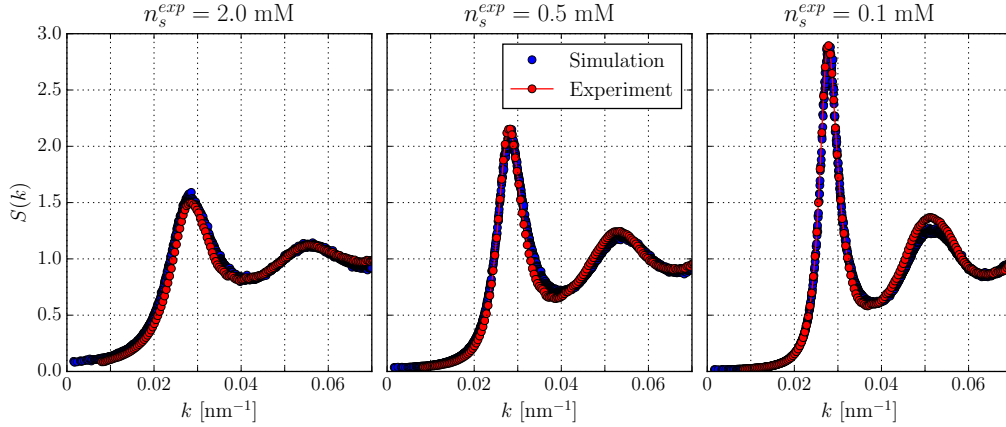


**Figure 9:** Structure factors at volume fraction  $\phi^{\text{nom}} = 0.32$ .

If the density at a some distance to a particle is just the average, the structure factor will also be 1 since all interference that may come from some local alignments average out over the illuminated sample.

Salt concentration $n_s$	RMS
0.10	0.043
0.35	0.052
5.00	0.048

**Table 3:** RMS at volume fraction  $\phi^{\text{nom}} = 0.32$ .

Following this comparison, we proceed with investigating the dataset we've obtained for a similarly parametrized potential according to table 1.

## 3.2 Further investigation of local correlation

### 3.2.1 Radial distribution function

If we look at the radial distribution functions for different packing fractions, we can easily get an idea if the structure of the system is more than a simple liquid phase or not. For the volume fractions presented in figure 10 we see that there are 2, almost 3 neighbour shells and as the volume fraction increases, these shells move further in towards the particle because there is simply less space. The peak heights of the neighbour shells grow



for increasing volume fraction, suggesting a bigger inter particle correlation.

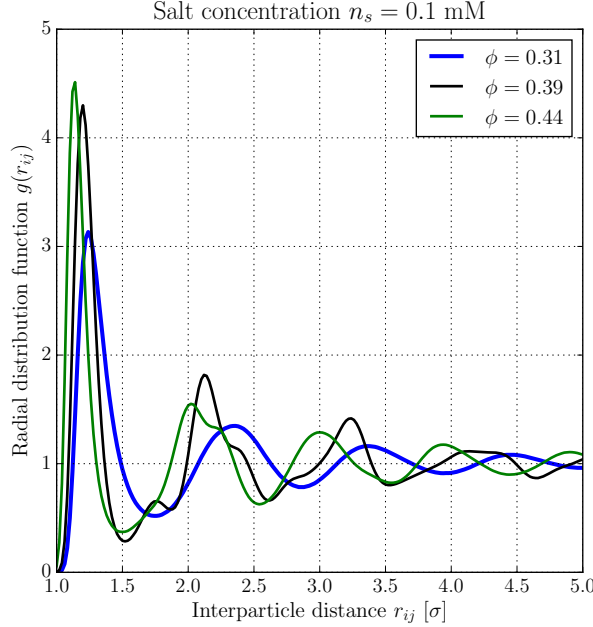


**Figure 10:** Structure factors at volume fraction  $\phi^{\text{nom}} = 0.32$ .

While the lowest volume fraction  $\phi = 0.31$  drawn in blue shows a simple oscillation, the higher volume fractions occur to have a more complex structure. For the next higher volume fraction  $\phi = 0.39$  there is a smaller peak in between the first to shells at a distance around  $1.75 \sigma$ . Also a shoulder on the second shell's peak appears at ca.  $2.4 \sigma$  and another one at ca.  $2.8 \sigma$ . This indicates more complex local alignments. We will discuss these cases in the next section, where we have additional information from the measurements of the bond orientational order.

At the largest shown volume fraction of  $\phi = 0.44$  for this salt concentration in green colour, the correlation has increased again in the first neighbour shell but decreased in the second and third one, indicating that the correlation length decreased. Also the structure that was present at lower packing shown in black fraction disappeared to some extent, at least the first additional peak. This is somehow surprising since one might think that correlation between particles will always increase with increasing volume fraction. But, one should note that, increasing the volume fraction is not similar to increasing the density. We have seen (e.g. fig. 2) that for increasing the volume fraction also the screening is increased.

For the lower salt concentration, we expect to get longer ranging correlation since the screening is less. Since the coupling is also stronger as can be seen in fig. 2 we can also expect an increased correlation and more complex behaviour at lower volume fractions. Both can be seen in fig. 11. Again, we show a low volume fraction sample's RDF with less correlation, a sample's RDF at intermediate volume fraction that shows high correlation and a high volume fraction that shows less correlation as before. Compared to the higher screening the modulation of the RDF is much stronger and ranges more outward.

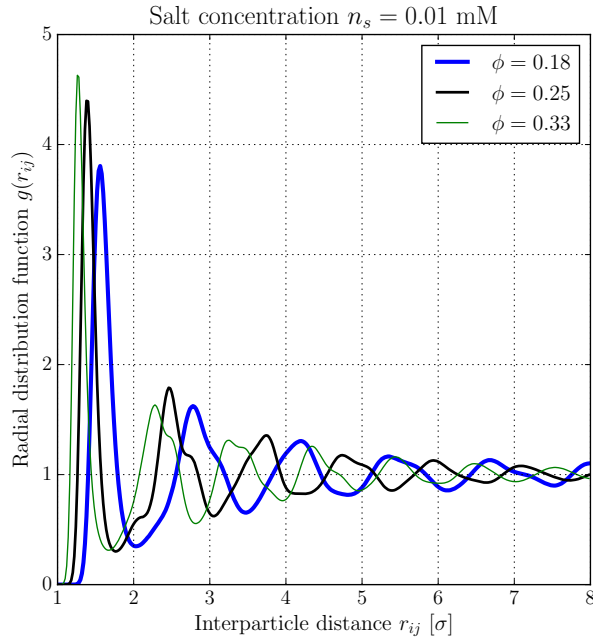


**Figure 11:** Structure factors at volume fraction  $\phi^{\text{nom}} = 0.32$ .

The fact that RDF still decays to unity for larger inter particle distances, tells us that we don't have any fully crystalline system.

#### 3.2.2 Bond orientational order

As mentioned before, we can compare the symmetries possessed by a particle's first neighbour shell with table values for perfect crystals as given in tab. 4.

For determining the local crystal structure according to the symmetry a particle's first neighbour shell has, a 2D scatter histogram with combined  $q_4$  and  $q_6$  information is necessary. Out of each generated configuration file for a state point we randomly select 200 particles. Dense scattering around a lattice's symmetry value combination indicates local crystal structures.

Crystal lattice	$q_4$	$q_6$
bcc	0.036	0.511
fcc	0.190	0.575
hcp	0.097	0.484

**Table 4:**  $q_4$  and  $q_6$  symmetry values for occurring ideal lattices [5].

Positive feedback in the  $c^l(ij)$  correlation measure indicates clustering. To investigate the correlation between particles, we draw a histogram of the  $c^l(ij)$  values. The  $q_4$  and  $q_6$  scattering plot and the histograms for its correlation  $c^l(ij)$  can be seen in fig. 12 and fig. 13, respectively. All the states are at higher screening of  $n_s = 0.1$  mM and correspond to the RDFs shown in fig. 10.

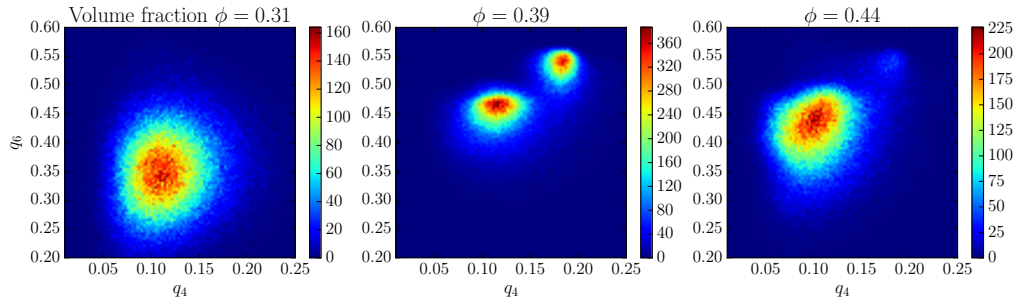


**Figure 12:** Scattering plot of  $q_6/q_4$  for different volume fractions  $\phi$  at salt concentration  $n_s^{\text{nom}} = 0.1$ . The scattering intensity is shown in colourcode.

For the lowest volume fraction, the RDF suggested a simple liquid phase. The symmetry shows a really broad scattering around a value that does not lie in the region of any crystal lattice's symmetry. Together with the histogram of  $c^l(ij)$  which doesn't show a sign of correlation, this tells that the system is liquid at  $\phi = 0.31$ .

The present systems have not shown an evidence of crystallinity in the RDF. So, one has to expect the bond order symmetries to deviate from the ideal ones in tab. 4. One should note that in [5], the nearest neighbours were calculated in a different manner than we do. We believe that should make very little difference in our results.

At  $\phi = 0.39$  shown in the middle panel in both plots we see scattering of the symmetry around two points that lie close to hcp and fcc symmetry. Also the  $c^l(ij)$ -histogram indicates that a large fraction is in a crystal-like

### 3.2 Further investigation of local correlation

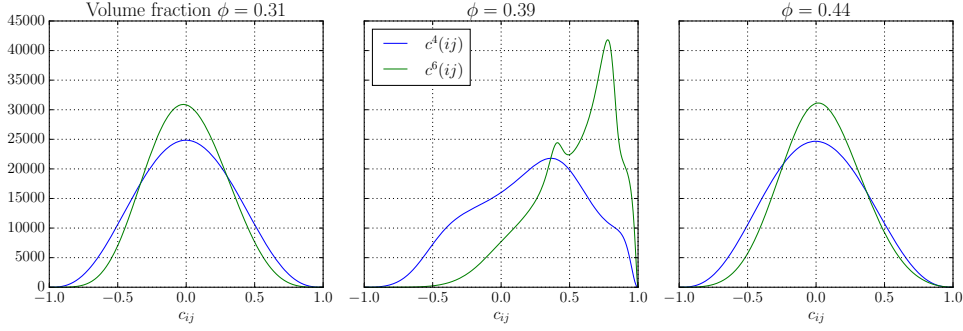


**Figure 13:** Plot of  $c^l(ij)$  for both symmetries, for different volume fractions  $\phi$  at salt concentration  $n_s^{\text{nom}} = 0.1$ . Blue:  $q_3$ . Green:  $q_4$ . Red:  $q_6$

state. There are two peaks appearing in the  $c^6(ij)$ -histogram which might belong to the to of the scattering centres.

At  $\phi = 0.44$  the scattering is now much broader and still around the hcp symmetry point, while there still is a faint scattering at the fcc symmetry. The  $c^6(ij)$ -histogram has a extremely weakly shift to positive correlation, which is most presumably not meaningful. Since we have seen the second neighbour shell having a shoulder in the RDF, this altogether indicates local structure in a liquid phase. The hcp symmetry possibly arises from the high volume fraction.

For the lower screening system a few more features appear. Now already in at the lowest packing fraction  $\phi = 0.18$  we see scattering around hcp and faintly fcc symmetries.

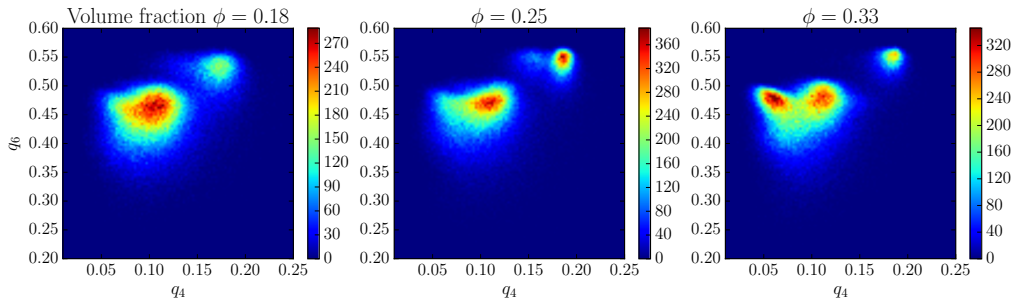


**Figure 14:** Scattering plot of  $q_6/q_4$  for different volume fractions  $\phi$  at salt concentration  $n_s^{\text{nom}} = 0.01$ .

As the volume fraction increases to  $\phi = 0.25$  we see a similar state as before at  $\phi = 0.39$  at screening  $n_s = 0.1$  mM, with a high correlation

and scattering around both hcp and fcc symmetries. At the highest shown  $\phi = 0.33$  in figure 14, there is a new symmetry of bcc occurring, being the strongest point that's scattered to. The  $c^6(ij)$ -histogram indicates positive correlation but very smeared out and does not exhibit a distinct peak.

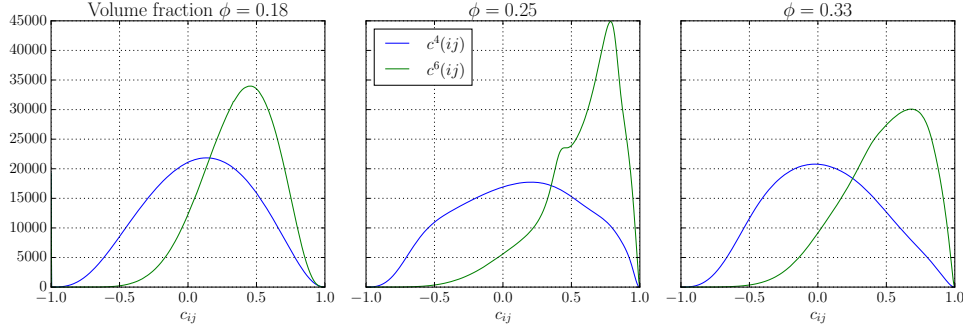


**Figure 15:** Plot of  $c^l(ij)$  for both symmetries, for different volume fractions  $\phi$  at salt concentration  $n_s^{\text{nom}} = 0.01$ . Blue:  $q_3$ . Green:  $q_4$ . Red:  $q_6$

Going to volume fraction higher than  $\phi = 0.33$  in the  $n_s = 0.01$  mM model, the correlation decays again as for the higher screening model. Again the hcp symmetry stays present, but the correlations completely decay as indicated by  $c^6(ij)$ .

### 3.3 Structure factor

After having seen the local structure with both real space symmetry measures of the RDF and the BOO parameters, we want to investigate our system in reciprocal space by calculating the structure factors, which can be directly determined via X-ray experiments. Figure 16 shows structure factors obtained for the higher screened potential.

In the leftmost figure showing  $\phi = 0.31$  the system was liquid and also the structure factor is that of a liquid. It is smoothly varying and decaying to large momentum transfer. Compared to fig. 6 for lower  $\phi = 0.16$  the second peak is not completely round indicating some more symmetry. In the middle we saw the the system to be correlated in both inter particle distances and bond orientational order. Added to the weak scattering of the liquid, we see high peaks like in a crystal, decaying quickly towards higher momentum transfer though, indicating only short ranged correlation. At volume fraction  $\phi = 0.44$  the system is less correlated in terms of distances. There is BOO but it is not correlated between particles. The sharp peak in the RDF produces a sharp peak in the structure factor. In the second peak of the structure factor we see faint peaks that might arise from the BOO

### 3.3 Structure factor

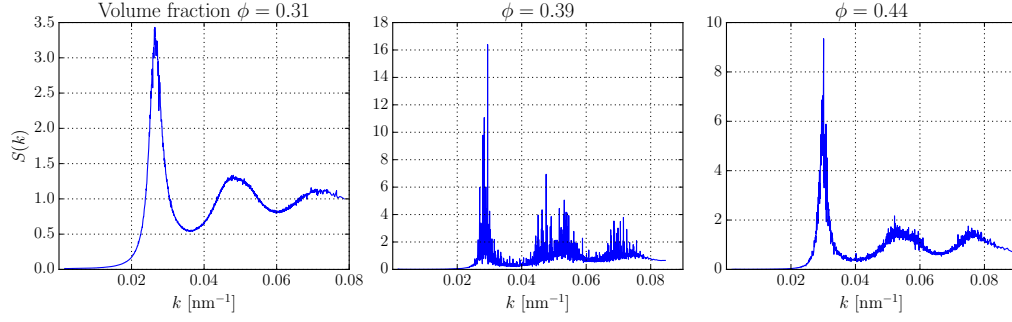


**Figure 16:** Structure factor, for different volume fractions  $\phi$  at salt concentration  $n_s^{\text{nom}} = 0.1$ .

and still high distance correlation.

In the less screened system the behaviour is similar. At  $\phi = 0.18$  we see the short ranged correlation producing high peaks in the structure factor on top of a liquid-like curve. The inter particle BOO correlation also vanished at higher volume fractions starting at  $\phi = 0.35$ , and again the structure factor becomes more like a typical liquid one. Strong local distance correlation to the first neighbour shell results in high first peaks in the corresponding structure factors.

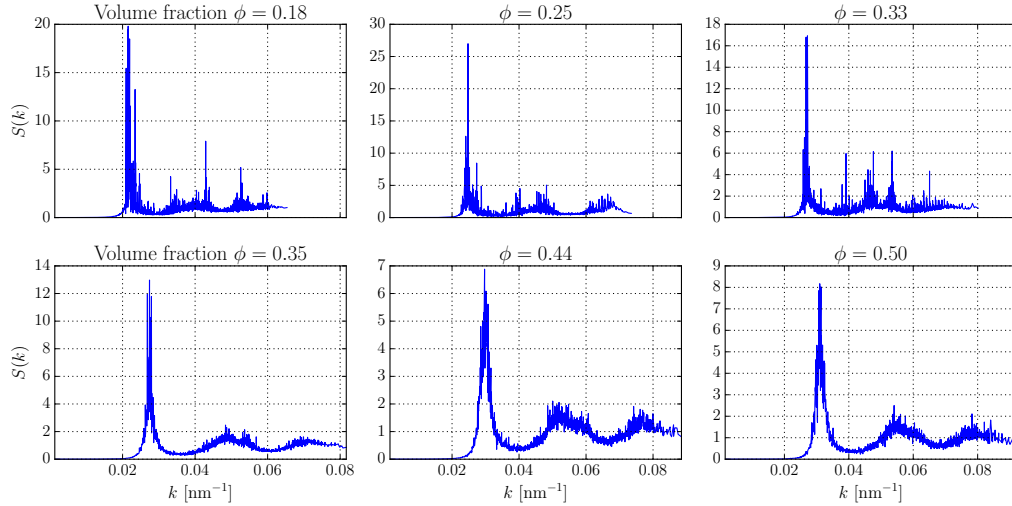


**Figure 17:** Structure factor, for different volume fractions  $\phi$  at salt concentration  $n_s^{\text{nom}} = 0.01$ .

## 4 Conclusion and outlook

Charge stabilised colloidal suspensions are a challenging system to investigate, using both simulations and experiments, as the non-trivial relationship between the volume fraction and screening results in interesting structural properties. The agreement between the analytically-derived results from DLVO theory, Monte Carlo simulations using the hard-core Yukawa potential model and the X-ray experiments on charge stabilised colloids, makes this model a very good candidate to go beyond understanding the structural properties via translational order parameters towards also including orientational order parameters. Thus, this model serves as a reasonable starting point for the investigation of how local BO parameters are related to results from angular cross-correlations (XCCA).

The RDF analysis proves to be useful when combined with a further analysis of BO parameters and the corresponding correlation functions  $c_{ij}^l$ . We observe that the hard-core Yukawa model fluid exhibits a rich phase diagram.

There are highly correlated fluid states that exhibit the BOO symmetries of different crystal lattices in their first neighbour shell at the same time. Additional to fluid states that showed non significant BOO, there are fluid states that exhibit high correlation, though only in the first neighbour shell.

While our model was monodisperse, the production of corresponding real colloids results in particles being both disperse in size and charge. One of the next steps following this work will therefore be including polydispersity in the model. This will be a significant step towards modelling experimental systems since polydispersity can have huge impacts on the crystalline (or aggregation) behaviour of the colloidal system [7].

Concluding, I learnt a lot about complex' liquids states and computing during my time at DESY. Special thanks to Avni Jain for selecting me for the summer student program, being my supervisors and helping me so much. Many thanks to the group for all the nice lunches, barbecue, and coffees we had. Also, many thanks to Felix Lehmkuhler, Lisbeth Janssen, Michael Hölting and Wojciech Roseker for many fruitful conversations and tips.

---

## References

- [1] Marco Heinen, Peter Holmqvist, Adolfo J Banchio, and Gerhard Nägele. Pair structure of the hard-sphere yukawa fluid: An improved analytic method versus simulations, rogers-young scheme, and experiment. *The Journal of chemical physics*, 134(4):044532, 2011.
- [2] M. P. Allen and D.J. Tildseley. *Computer Simulations of Liquids*. Calrendon Press, 1987.
- [3] Jean-Pierre Hansen and Ian R McDonald. *Theory of simple liquids*. Elsevier, 1990.
- [4] Kai Zhang. On the concept of static structure factor. *arXiv preprint arXiv:1606.03610*, 2016.
- [5] Walter Mickel, Sebastian C Kapfer, Gerd E Schröder-Turk, and Klaus Mecke. Shortcomings of the bond orientational order parameters for the analysis of disordered particulate matter. *The Journal of chemical physics*, 138(4):044501, 2013.
- [6] Fabian Westermeier, Birgit Fischer, Wojciech Roseker, Gerhard Grübel, Gerhard Nägele, and Marco Heinen. Structure and short-time dynamics in concentrated suspensions of charged colloids. *The Journal of chemical physics*, 137(11):114504, 2012.
- [7] Marjolein N van der Linden, Alfons van Blaaderen, and Marjolein Dijkstra. Effect of size polydispersity on the crystal-fluid and crystal-glass transition in hard-core repulsive yukawa systems. *The Journal of chemical physics*, 138(11):114903, 2013.